International Journal of Heat and Mass Transfer 52 (2009) 3994–4000

Contents lists available at ScienceDirect

International Journal of Heat and Mass Transfer

journal homepage: www.elsevier.com/locate/ijhmt

Energy separation in the wake of a cylinder: Effect of Reynolds number and acoustic resonance

K.S. Kulkarni [1], R.J. Goldstein *

Heat Transfer Laboratory, Department of Mechanical Engineering, University of Minnesota, 111 Church St. SE, Minneapolis, MN 55455, USA

ARTICLE INFO

Article history:
Received 16 November 2008
Accepted 23 March 2009
Available online 15 May 2009

Keywords:
Energy separation
Acoustic excitation
Wake of cylinder
Low Mach number
Flow reversal

ABSTRACT

Energy separation is a spontaneous redistribution of total energy in a flowing fluid without external work or heat transfer. The energy separation mechanism in the vortex field behind an adiabatic circular cylinder in a cross flow of air is investigated. Time-averaged velocity and temperature measurements taken one diameter downstream of the cylinder ($Re \sim 10^5$, $M_\infty \sim 0.25$) indicate flow reversal. The measured recovery temperature, expressed as distribution of energy separation factor indicates that energy separation is caused by the vortex flow in the wake, enhanced by acoustic excitation, and is insensitive to Reynolds number in the sub critical range studied.

1. Introduction

Since energy separation was first observed inside a vortex tube by Ranque [1], it has been studied for various flow situations: laminar and turbulent boundary layers [2,3], resonance tubes [4], shear layers [5], free jet flows [6–8], impinging jets [9–11] and vortex streets behind bluff bodies [12–14]. In case of free jets and flow behind bluff bodies, it is commonly believed that unsteady moving vortices cause energy separation.

1.1. Mechanism of energy separation

Eckert [15] explained the existence of energy separation with a model of a clockwise rotating vortex being convected from left to right. It consists of a viscous vortex core and an inviscid outer region. As shown in Fig. 1, the swirling velocity of the vortex is V_w and the convective velocity is V_0. The dimensionless total temperature inside the vortex is $(C_p(T_t - T_{t,\infty})/V_0V_w)$, where $T_{t,\infty}$ is the total temperature far away from the vortex center. Thus, the total temperature in the upper half of the vortex is greater than $T_{t,\infty}$ and it is lower than $T_{t,\infty}$ in the case of lower half. Fig. 1 shows the velocity pattern and isotherms for the flow around such a vortex. The total temperature maxima are located at the vortex extrema.

A similar model based on the energy equation for inviscid flow without conduction was proposed by Kurosaka et al. [16] (Eq. (1)). Two important points of this model are – (a) the total temperature follows the instantaneous fluctuations in pressure as seen in Eq. (1). (b) The pressure in the center of vortex is lower than outside.

$$\rho C_p \frac{DT_t}{Dt} = \rho \frac{Dh_t}{Dt} = \frac{\partial p}{\partial t} \tag{1}$$

Hence the total temperature of a fluid element following a trochoidal-like path in a vortex street (Fig. 2) starts to fall as it moves from 12 o'clock to 6 o'clock position since the fluid element is approached by the low pressure vortex center. As the vortex passes by the fluid element (6 o'clock–12 o'clock), the pressure rises in the second half of the cycle, raising the total temperature.

These mechanisms are supported by numerical and experimental studies by Han and Goldstein [6,7] and Seol and Goldstein [8] for the case of free jets. The authors measured energy separation factor in the far wake of a cylinder ($3 < x/D < 10$) for a fixed Reynolds number [14] and found that the moving vortex street causes lower total temperature near the wake centerline and higher total temperature near the wake limits.

1.2. Flow reversal in the near wake of cylinder

The flow over a circular cylinder forms an unsteady laminar wake at a relatively low Reynolds number ($Re \sim 48$) [17]. Beyond this Re, vortices are shed in the wake of the cylinder at a nearly constant non dimensional frequency, $St = fD/U_\infty$. Numerical and experimental works [18–22] suggest a $St \sim 0.2$ for $50 \leqslant Re \leqslant 2.0 \times 10^5$. At this Re, a laminar boundary layer forms on the front

* Corresponding author. Tel.: +1 612 625 5552.
E-mail addresses: kaustubh@me.umn.edu (K.S. Kulkarni), rjg@me.umn.edu (R.J. Goldstein).
[1] Tel.: +1 612 306 3082.

0017-9310/$ - see front matter © 2009 Elsevier Ltd. All rights reserved.
doi:10.1016/j.ijheatmasstransfer.2009.03.024

Nomenclature

English

C_p	specific heat at constant pressure for the fluid [J/Kg K]
D	diameter of circular cylinder [m]
f	frequency of vortex shedding [Hz]
$\dot{H}_{d,\infty}$	enthalpy flow (Eq. (8)) [W]
$\Delta\dot{H}_t$	difference in enthalpy flow between upstream and downstream of cylinder (Eq. (7)) [W]
h_t	stagnation enthalpy per unit mass of fluid [J/Kg]
M_∞	free stream Mach number
$\dot{m}$	mass flow rate at downstream location (x/D = 1) [Kg/s]
$\dot{m}_0$	mass flow rate at upstream location (x/D = −20) [Kg/s]
p	static pressure of fluid [Pa]
Re	Reynolds number ($Re = U_\infty D/\nu$)
r	recovery factor of temperature probe
S	energy separation factor (Eq. (3))
St	Strouhal number ($St = fD/U_\infty$)
T_d	local dynamic temperature (Eq. (4)) [K]
$T_{d,\infty}$	dynamic temperature ($= U_\infty^2/2C_p$) [K]
$T_{d,00}$	dynamic temperature in absence of cylinder ($= U_{00}^2/2C_p$) [K]
T_r	recovery temperature measured by the probe [K]
$T_{r,00}$	recovery temperature measured by the probe in absence of cylinder [K]
T_t	total (stagnation) temperature [K]
$T_{t,\infty}$	total (stagnation) temperature at wind tunnel inlet [K]
t	time [s]
U	instantaneous streamwise velocity [m/s]
$\overline{U}$	time-averaged streamwise velocity [m/s]
$\overline{U}_0$	time-averaged streamwise velocity at upstream location (x/D = −20) [m/s]
U_{00}	streamwise velocity in the absence of cylinder [m/s]
U_∞	spatially and temporally averaged streamwise velocity at upstream location (x/D = −20) (Eq. (5))[m/s]
$\langle\overline{U}\rangle$	spatially and temporally averaged streamwise velocity (Eq. (6)) [m/s]
u'	random fluctuations in streamwise velocity (X direction) [m/s]
V_0	convective velocity of vortex [m/s]
V_w	swirling velocity of vortex [m/s]
v'	random fluctuations in cross-stream velocity (Y direction) [m/s]
W	width of test section [m]
w'	random fluctuations in span wise velocity (Z direction) [m/s]
X	streamwise direction
x	distance in streamwise direction from center of the cylinder [m]
Y	cross-streamwise direction
y	distance in cross-streamwise direction from the center of the cylinder [m]
Z	span wise direction

Greek

ρ	fluid density [Kg/m^3]
θ	angle measured from front stagnation line of the cylinder [°]

of the cylinder surface and flow reversal takes place at $\theta > 90°$. The flow in the far wake of the cylinder is a close approximation of von Karman vortex street described in the models of Eckert [15] and Kurosaka et al. [16]. However, the flow close to the cylinder ($x/D \leqslant 2$) is strongly affected by the cylinder surface and a time-averaged flow reversal is observed. Owen and Johnson [23] using LDV measured the mean and turbulent velocity in the near wake of a cylinder for $Re = 1.67 \times 10^5$, $M_\infty = 0.6$. The time-averaged measurements show the mean flow reversal in the region $x/D \leqslant 1.3$ with a reverse flow velocity of 25% of U_∞ at $x/D = 1$. Numerical solutions by Catalano et al. [24] using LES and RANS for $Re = 1 \times 10^6$, show 25% reverse flow velocity at $x/D = 0.75$ and no reverse flow at $x/D = 1.5$, supporting the measured [23] limit on the extent of reverse flow region.

1.3. Energy separation in the flow around a cylinder – effect of acoustic excitation

Eckert and Weise [2] first observed energy separation on the surface of a cylinder in cross flow for $Re = 1.4 \times 10^5$, $M_\infty = 0.685$. The existence of energy separation was confirmed by Ryan [25] in the wake of a cylinder. In addition, he found that when the frequency of vortex shedding resonated with the first harmonics of

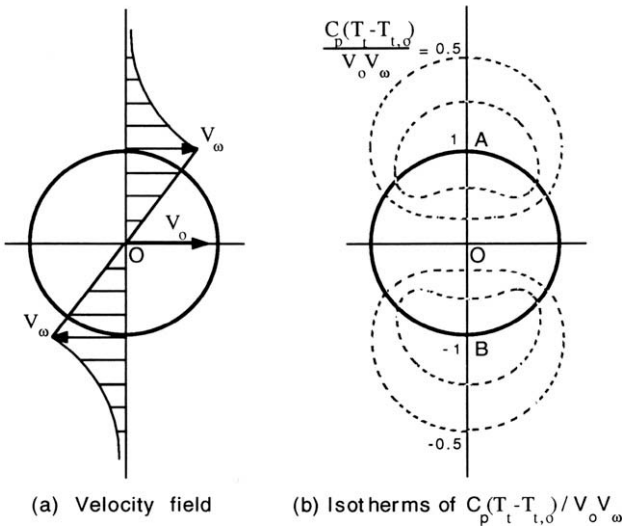

Fig. 1. Velocity field and total temperature distribution near a vortex [15].

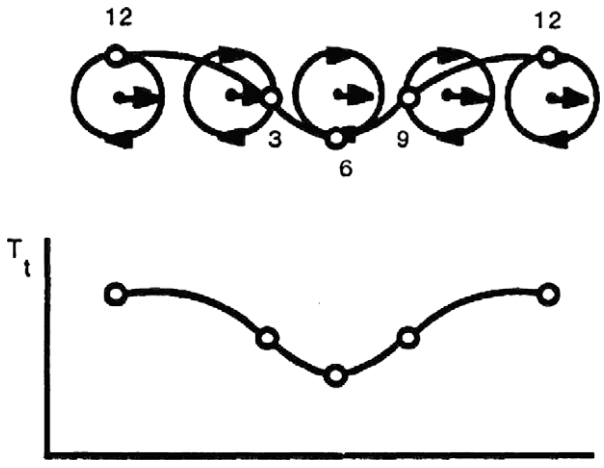

Fig. 2. Variation of total temperature along a path line in a vortex street [16].

the test section, confirmed by a loud noise; energy separation effect was enhanced on the cylinder surface. Goldstein and He [12] measured instantaneous velocity and temperature in the near wake of a cylinder and showed positive correlation between enhanced vortex strength due to acoustic excitation and energy separation effect. Kurosaka et al. [16] showed that different modes of the standing wave in span wise direction can be excited selectively by adjusting the vortex shedding frequency, giving rise to stronger or weaker energy separation effect at span wise different locations. The effect of acoustic excitation is confirmed for free jets by Han and Goldstein [7] using radially directed speakers to excite the jet flow. Instantaneous measurements of pressure and temperature show that vortex pairing process induced by acoustic excitation results in stronger energy separation. This supports the hypothesis that moving vortices cause energy separation.

1.4. Present work

Few direct measurements of energy separation in the wake of a cylinder are available that explore the effect of acoustic excitation. Some are restricted to supersonic or transonic flows. The mechanisms proposed by Eckert [15] and Kurosaka et al. [16] imply that energy separation is evident and measurable in a low Mach number flow. Earlier, the authors have reported energy separation measurements in the far wake ($3 < x/D < 10$) of a cylinder at a fixed Reynolds number, not corresponding to acoustic excitation [14]. Hence, the objectives of the present study are:

1. Verify the existence of energy separation in the near wake of cylinder ($x/D < 3$) at low Mach number flows ($0.22 \leqslant M_\infty \leqslant 0.25$).
2. Study effect of acoustic excitation by coupling vortex shedding frequency with the test section natural frequency.
3. Study effect of Reynolds number variation on energy separation in the subcritical range.

2. Experimental apparatus and procedure

2.1. Experimental facility

The details of the experimental facility are described in [14]. A short description is provided here. A suction-type subsonic wind tunnel is used in the present study. It has a bell-mouth inlet of 609 mm × 609 mm cross sectional area that allows air to enter the tunnel through a series of wire mesh screens placed 100 mm apart to reduce the free stream turbulence. Two flow contractions having area ratios 9:1 and 5:3, downstream of the screens, lead to the test section. The air speed (up to 95 m/s with no obstruction in test section) obtained with this section provides the dynamic temperature of ~4.5 K.

The test section is a 1346 mm long rectangular duct made of 19 mm thick Plexiglas sheets with a cross section of 120 mm (height) × 203 mm (width) (Fig. 3a). Two test windows 305 mm × 127 mm, on top and bottom walls of the duct allow insertion of the vertical test cylinder. Two slots – 300 mm long × 5 mm wide and 50 mm apart are cut through a side wall for insertion of temperature and hot wire probes. The vertical adiabatic test cylinder (Fig. 3b) made of phenolic has a 19 mm OD and that results in a 9.4% blockage in the test section.

2.2. Recovery temperature probe

A bare wire thermocouple probe (Fig. 4), based on design ideas by Hottel and Kalitinsky [26] and Moffat [27] is used to determine the total temperature in the flow. It consists of a butt-joint welded

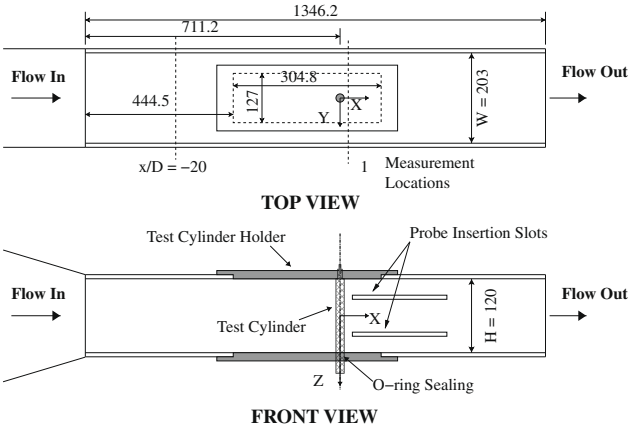

(a) Schematic Diagram of Test Section (All Dimensions in mm)

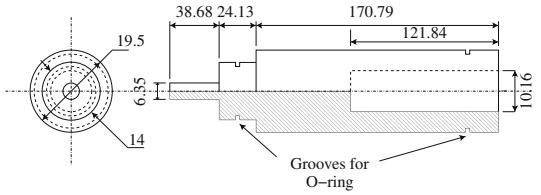

(b) Schematic Diagram of Test Cylinder (All Dimensions in mm)

Fig. 3. Schematic diagram of test apparatus.

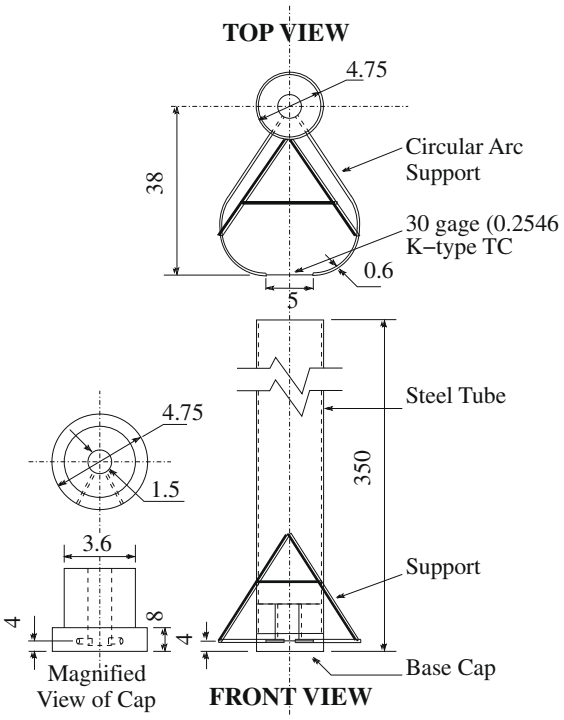

Fig. 4. Schematic diagram of recovery temperature probe (all dimensions in mm).

K-type thermocouple made from 30 gage insulated wires supported by circular arc tubes as shown in Fig. 4. It has successfully measured total temperature and hence, energy separation factor in the far wake ($x/D > 3$) of a cylinder [14].

2.3. Experimental procedure

An automated traversing system mounted on the side wall of the test section moves the recovery temperature and hot wire

probes at desired streamwise locations ($x/D = -20$ and 1). A Centroid motion controller controlled by a Linux workstation operates a stepper motor to achieve a smallest displacement of 6.25 μm. The details of the setup are described in [14]. The automated traverse can span the entire width (203 mm) of the test section, but the motion is restricted to −96 mm to + 70 mm with respect to the axis of the cylinder due to structural constraints on the temperature probe. The probes are moved in steps of 2 mm, resulting in 84 measurements at each x/D location.

The recovery temperature probe is calibrated at different air speeds to assess its accuracy and consistency in measuring the recovery temperature in the flow. The recovery factor,

$$r = 1 + \frac{T_{r,00} - T_{t,\infty}}{U_{00}^2/2C_p} = 1 + \frac{T_{r,00} - T_{t,\infty}}{T_{d,00}} \quad (2)$$

is determined by measuring the recovery temperature of the probe in the tunnel ($T_{r,00}$) for a known flow velocity using a pitot tube near the probe (U_{00}) and total temperature ($T_{t,\infty}$) from five thermocouples placed at the inlet of the wind tunnel. The calibration is done in the absence of the test cylinder. The recovery factor is found to be nearly constant (0.735 ± 0.02) for the tested range of free stream velocity (65–95 m/s) and is shown in Fig. 5.

Velocity and temperature measurements are taken simultaneously with hotwire velocity and recovery temperature probes inserted through two slots in the side wall of the test section (Fig. 3a). Interchanging the probe positions between these two slots, it is concluded that the flow is two dimensional with negligible variation with the span wise (vertical) position. When the recovery temperature probe is moved in the wake of the cylinder, the total temperature of the flow measured at wind tunnel inlet using five thermocouples is continuously monitored. This reference total temperature is used to calculate the energy separation factor at each location of the recovery temperature probe. Hotwire measurements are used to obtain the instantaneous velocity which is used to calculate time-averaged velocity ($\overline{U}$) and random fluctuations u' and v'. An impact tube is used to verify the hotwire measurements in the region of flow reversal ($x/D = 1$). Due to the close proximity of the cylinder, it is not possible to make velocity measurements in the flow reversal region with the impact tube facing downstream. Hence, the measurements are forced to 0 m/s in this region. Due to directional (±) insensitivity of the hotwire, its measurements are forced to negative values based on the impact tube indication of flow reversal (Fig. 6). The turbulence intensity ($(u'^2 + v'^2)^{0.5}/\overline{U}$) upstream of the cylinder at $x/D = -20$ is ~0.2%.

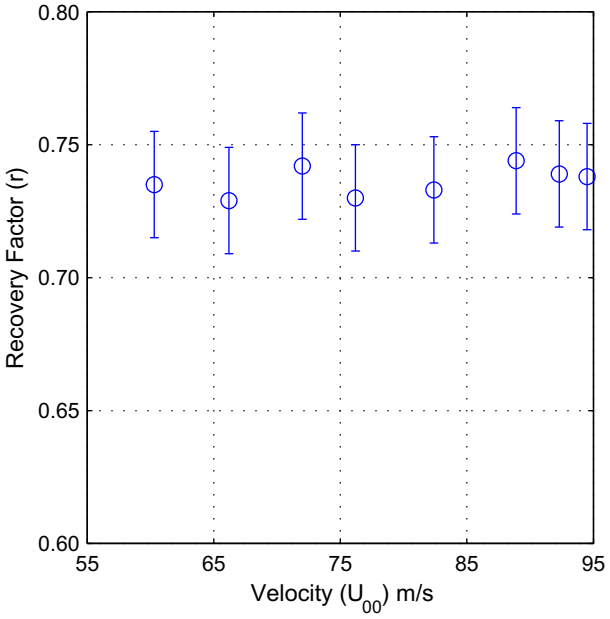

Fig. 5. Calibration of recovery temperature probe [14].

3. Results and discussion

3.1. Data reduction procedure and calculations

The time-averaged total temperature in the wake of the cylinder is normalized by the upstream dynamic temperature and expressed as energy separation factor (S).

$$S = \frac{T_t - T_{t,\infty}}{T_{d,\infty}} = \frac{T_r + (1-r)T_d - T_{t,\infty}}{T_{d,\infty}} \quad (3)$$

where,

$$T_d = \frac{\overline{U}^2}{2C_p} = \frac{(\overline{U}^2 + \overline{u'^2} + \overline{v'^2})}{2C_p} \quad (4)$$

The local average dynamic temperature (Eq. (4)) is obtained from hotwire velocity measurements for every cross-stream (y/D) location. Velocity fluctuations (w') in the span wise Z direction are found to be negligible [14]. Local dynamic temperature is substantially altered by the turbulent fluctuations and a detailed discussion of this effect of turbulence on energy separation factor has been given [14]. The energy separation factor has an overall uncertainty of ±0.021. The uncertainty is not expressed as percentage since the typical value of S is close to 0. This uncertainty corresponds to 2.3% of the maximum value of S observed at rear stagnation line.

3.2. Mass and enthalpy balance

The measurement validity is examined by performing both mass and enthalpy flow balances across the measurement planes. Spatially and temporally averaged velocities evaluated at $x/D = -20$ and 1, respectively, are defined as U_∞ and $\langle\overline{U}\rangle$ (Eqs. (5) and (6)).

$$U_\infty = \frac{1}{W}\int_{-W/2}^{W/2} \overline{U}_0 dy \text{ at } X/D = -20 \quad (5)$$

$$\langle\overline{U}\rangle = \frac{1}{W}\int_{-W/2}^{W/2} \overline{U} dy \text{ at } X/D = 1 \quad (6)$$

U_∞ is used to normalize the downstream time-averaged velocity ($\overline{U}$) in Figs. 6 and 8. The total enthalpy difference between the upstream and downstream locations ($\Delta\dot{H}_t$, defined in Eq. (7)) is normalized by the enthalpy of the flowing mass with the dynamic temperature of the free stream ($\dot{H}_{d,\infty}$, defined in Eq. (8)). The normalization enthalpy represents the maximum energy that can be distributed within the fluid as a result of energy separation.

$$\Delta\dot{H}_t = \int \dot{m}_0 C_p (T_{t,0} - T_{t,\infty}) dy|_{X/D=-20} - \int \dot{m} C_p (T_t - T_{t,\infty}) dy|_{X/D=1} \quad (7)$$

$$\dot{H}_{d,\infty} = \int \dot{m}_0 C_p T_{d,\infty} dy \quad (8)$$

Details of this procedure can be found in [14]. Table 1 shows the mass and enthalpy balance results at $x/D = 1$ for all the Reynolds numbers. The mass balance and enthalpy balance are found to be within 7% and 52%, respectively. The moderate accuracy of hotwire velocity probe in the reverse flow region and the choice of normalization enthalpy can be attributed to such poor mass and energy balance. However, very good results obtained for downstream

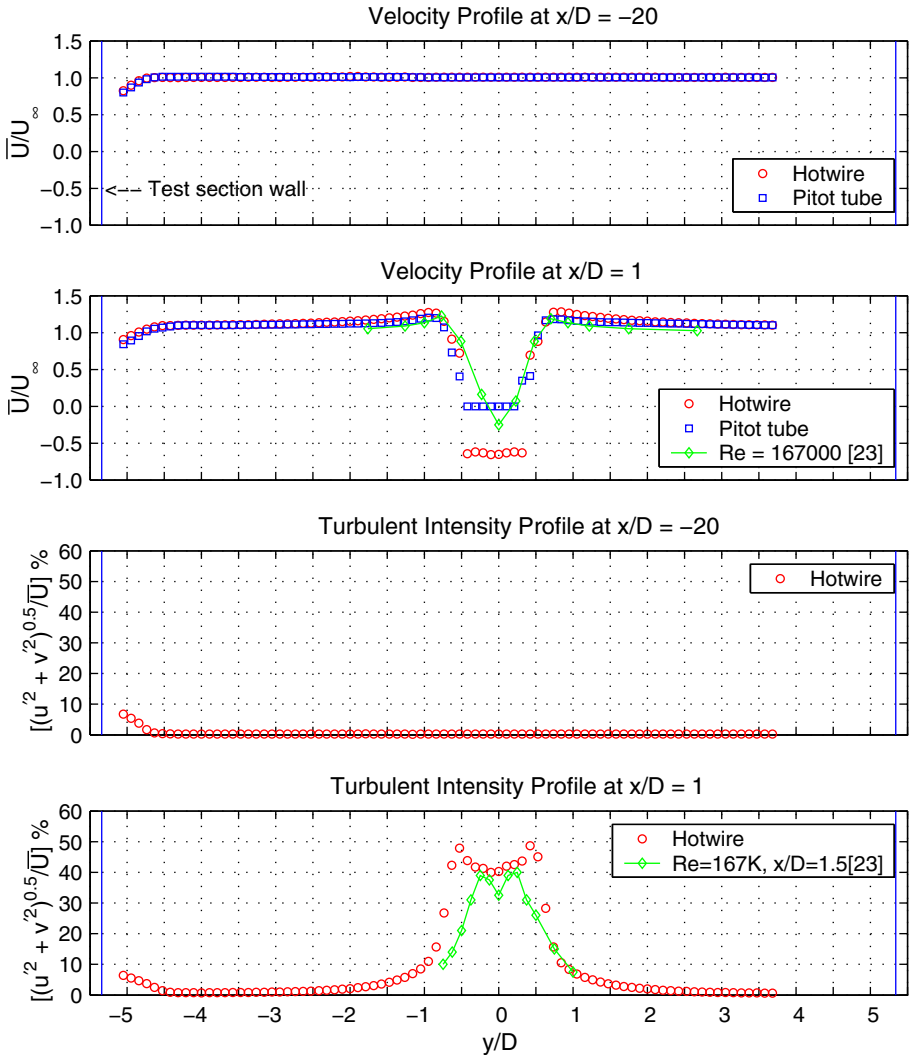

Fig. 6. Normalized velocity and turbulent intensity profile (Re = 92,000).

Table 1
Summary of mass and energy balance at $x/D = 1$.

Re	$\frac{\overline{U}}{U_\infty}$		$\frac{\Delta \dot{H}_r}{\dot{H}_{d,\infty}}$ (%)
	Hotwire (%)	Pitot tube (%)	
92,000	93.5	96.5	−52.26
99,000	94.9	–	38.36
106,000	100.2	–	−13.54

locations ($x/D > 3$) shown in [14] validate the measurement technique used in the present work.

3.3. Velocity measurements – reverse flow region

The mean velocity measurements performed with hotwire and impact tube for the case of $x/D = 1$ and Re = 9.2×10^4 are presented in Fig. 6. Results from Owen and Johnson [23] obtained with LDV are also included for comparison. Some important factors that can be noted from these results are:

1. The hotwire and impact tube measurements for mean velocity compare well with Owen and Johnson [23] showing a central reverse flow region sandwiched between accelerated flow regions in the outer wake. Turbulent intensity measurements in the present study agree well with Owen and Johnson [23] measurements.
2. Hotwire measurements tend to overestimate the velocity in the wake region due to the insensitivity of hotwire to flow direction. The curve deviates from the impact tube measurements near the outer wake region. Also, the reverse flow velocity is found to be higher (more negative) and much flatter velocity distribution is seen in contrast to a smoother distribution obtained using LDV [23].
3. The impact tube measurements indicate a flow reversal region between $-0.5 \leqslant y/D \leqslant 0.5$, whereas LDV measurements [23] and LES, RANS computational simulations [24] indicate a smaller reverse flow region with lower magnitude of reverse velocity. The overestimation of reverse flow region is attributed to a moderate accuracy of impact tube and hotwire measurements in the reversal region.
4. The time-averaged turbulent intensity at $x/D = 1$ in the present case and $x/D = 1.5$ in the case of Owen and Johnson [23] compare favorably showing high turbulent intensity regions near the outer wake. This high turbulent intensity contributes significantly to the dynamic temperature (Eq. (4)) and hence, the energy separation factor.

3.4. Energy separation – effect of Reynolds number (non-acoustic excitation case)

Fig. 7 shows the time-averaged energy separation factor calculated at $x/D = 1$ for Re = 9.2×10^4 and 1.06×10^5. The profiles show the presence of energy separation in the wake of the cylinder. A central region of large negative S is sandwiched between two positive S peaks near the outer wake limits. This observation disagrees with the prediction of Kurosaka et al. [16]. They hypothesize as an explanation to their observation; that for time-averaged measurements, the path lines of two particles – one bound to the vortex on one side of the cylinder (similar to Fig. 2) and the other crossing over from one vortex on the other side neutralize the positive energy separation effect resulting in only a colder wake behind the cylinder. This path line cross over may occur in vortex streets which is the region of $x/D > 3$. Time-averaged energy separation measurements for $x/D > 3$ reported in [14] support this hypothesis. However, at $x/D = 1$, such a cross over may not occur due to the flow circulation in the wake center at this Re.

It can be also noted from Fig. 7 that in the range studied, the Reynolds number has no significant effect on the energy separation factor distribution and the two profiles are identical within the uncertainty of the measurement.

3.5. Energy separation – effect of acoustic excitation

When the frequency of vortex shedding matches with the fundamental frequency (or its integral multiple) of standing wave in the wind tunnel test section, the flow resonates and a shrieking noise is heard during the experiments. Such an acoustically excited flow condition occurs at Re = 9.9×10^4 in the present study. Fig. 8 shows a comparison of mean velocity and turbulent intensity profiles measured at $x/D = 1$ for Re = 9.9×10^4 and 1.06×10^5, a non-resonant case. The velocity measurements indicate that the time-averaged flow structure is unaffected by the acoustic excitation. The energy separation factor distribution for the two cases, however, shows considerable difference as seen in Fig. 9. Both the positive and negative energy separation magnitudes are larger for the resonance case confirming earlier observations by Ryan

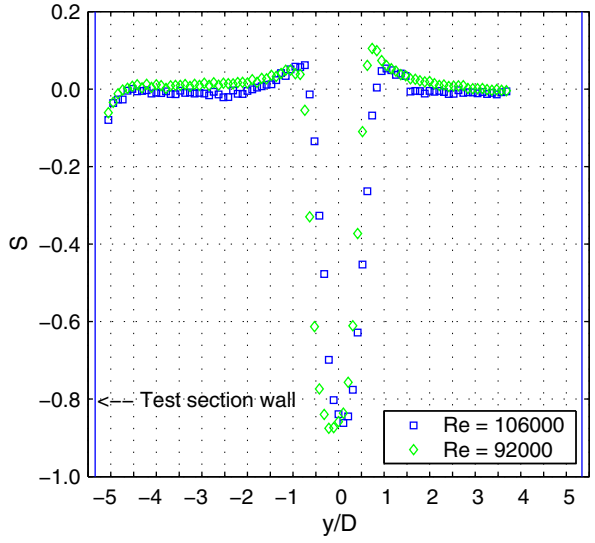

Fig. 7. Effect of Reynolds number on energy separation factor profile at $x/D = 1$.

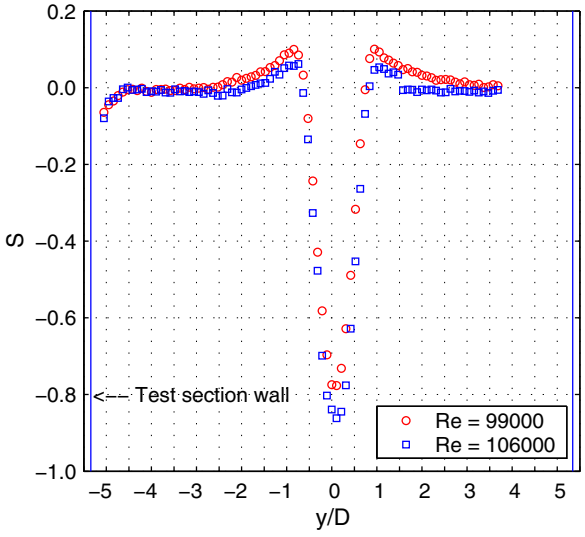

Fig. 9. Effect of acoustic excitation on energy separation factor profile at $x/D = 1$.

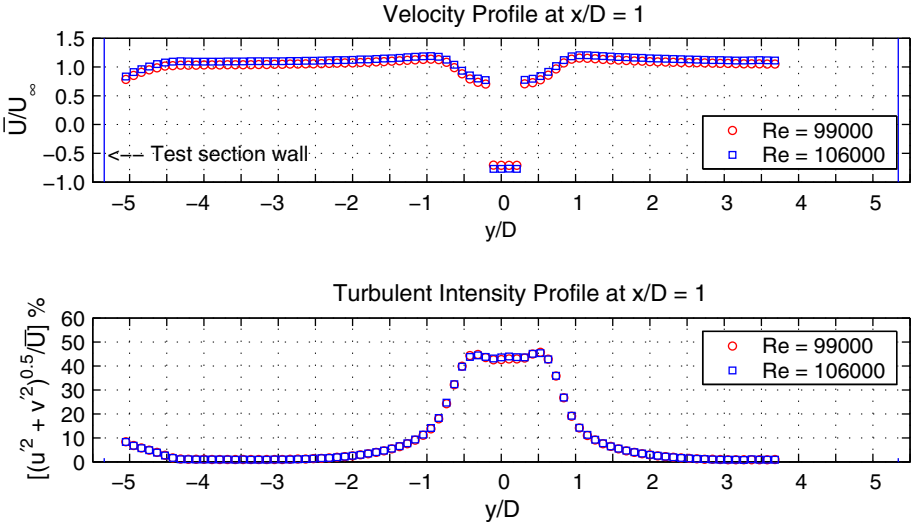

Fig. 8. Effect of acoustic excitation on mean flow measurements at $x/D = 1$.

[25], Goldstein and He [12] and Kurosaka et al. [16]. Acoustic excitation increases the vortex strength which is manifested in higher energy separation effects confirming that the vortical structures are the cause of energy separation as presented by Eckert [15] and Kurosaka et al. [16].

4. Conclusions

Time-averaged velocity and total temperature are measured in the mean wake behind a circular cylinder to study the phenomenon of energy separation. Flow at one Reynolds number studied corresponds to the resonance between the vortex shedding and the wind tunnel acoustics resulting in acoustically excited flow. The following conclusions can be drawn based on the experimental results:

1. The measured energy separation factor (S) profiles indicate the presence of energy separation in the wake of cylinder even at low Mach numbers and in time-averaged flow.
2. Large negative energy separation is observed near the wake centerline and significant positive energy separation is observed in the outer wake for the time-averaged measurements. It indicates that the positive energy separation neutralization due to time averaging does not occur in the near wake.
3. Acoustic excitation increases the overall energy separation effect. Since instantaneous velocity measurements have shown increased vortex strength for acoustically excited flow [7,12,16], it can be concluded that the unsteady vortical structures are the cause of energy separation as presented by Eckert [15] and Kurosaka et al. [16]. The time-averaged flow structure for an acoustically excited case however, is found to be similar to an acoustically non-excited case.
4. For the range studied, energy separation effect appears to be independent of Reynolds number in the sub critical range for the non-acoustically excited cases.

References

[1] G. Ranque, Experiences sur la d'etente giratoire avec productions simultan/ees d'un echappement d'air chaud et d'un echappement d'air froid, Journal of Physics Radium 4 (1933) 112–114.
[2] E.R.G. Eckert, W. Weise, Messungn der Temperaturverteilung auf der Oberflache Schnell Angestromter umbeheizter korper, der Deutschen Luftfahrtforschung 2 (1940) 25–31.
[3] E.R.G. Eckert, O. Drewiz, Die Berechnung des Temperaturfeldes in der laminaren Grenzschicht schnell angestromter, unbeheizter Korper, Luftfartforschung 19 (1941) 189–196.
[4] E.R.G. Eckert, Energy Separation in Fluid Streams, International Communications in Heat and Mass Transfer 13 (1986) 127–143.
[5] B. Han, R.J. Goldstein, H.G. Choi, Energy separation in shear layers, International Journal of Heat and Mass Transfer 45 (2002) 47–55.
[6] B. Han, R.J. Goldstein, Instantaneous energy separation in a free jet. Part I. Flow measurement and visualization, International Journal of Heat and Mass Transfer 46 (21) (2003) 3975–3981.
[7] B. Han, R.J. Goldstein, Instantaneous energy separation in a free jet. Part II. Total temperature measurement, International Journal of Heat and Mass Transfer 46 (21) (2003) 3983–3990.
[8] W.S. Seol, R.J. Goldstein, Energy separation in a jet flow, Transactions of ASME, Journal of Fluids Engineering 119 (1) (1997) 74–82.
[9] R.J. Goldstein, A.I. Behbahani, K.K. Heppelmann, Streamwise distribution of the recovery factor and the local heat transfer coefficient to an impinging circular air jet, International Journal of Heat and Mass Transfer 29 (8) (1986) 1227–1235.
[10] R.J. Goldstein, K.A. Sobolik, W.S. Seol, Effect of entrainment on the heat transfer to a heated circular air jet impinging on a flat surface, Transactions of ASME, Journal of Heat Transfer 112 (1990) 608–611.
[11] M. Fox, M. Kurosaka, K. Hirano, Total temperature separation in jets, in: AIAA 21st Fluid Dynamics, Plasma Dynamics and Lasers Conference, Seattle, WA, 1990.
[12] R.J. Goldstein, B. He, Energy separation and acoustic interaction in flow across a circular cylinder, Transactions of ASME, Journal of Heat Transfer 123 (2001) 682–687.
[13] B.W. Van Oudheusden, Energy separation in steady separated wake flow, Transactions of ASME, Journal of Fluids Engineering 127 (3) (2005) 611–614.
[14] R.J. Goldstein, K.S. Kulkarni, Energy separation in the wake of cylinder, Journal of Heat Transfer 130 (6) (2008) 0617031–0617039.
[15] E.R.G. Eckert, Cross transport of energy in fluid streams, Warme und Stoffubertragung 21 (1987) 73–81.
[16] M. Kurosaka, J.B. Gertz, J.E. Graham, J.R. Goodman, P. Sundaram, W.C. Ringer, H. Kuroda, W.L. Hankey, Energy separation in a vortex street, Journal of Fluid Mechanics 178 (1987) 1–29.
[17] M.M. Zdravkovich, Flow Around Circular Cylinders: A Comprehensive Guide Through Flow Phenomena, Experiments, Applications, Mathematical Models and Computer Simulations, Oxford Science Publications, 1997.
[18] C.A. Friehe, Vortex shedding from cylinders at low Reynolds numbers, Journal of Fluid Mechanics 100 (1980) 237–241.
[19] B. Cantwell, D. Coles, An experimental study of entrainment and transport in the turbulent near wake of a circular cylinder, Journal of Fluid Mechanics 136 (1983) 321–374.
[20] L.E. Ericsson, J.P. Reding, Criterion for vortex periodicity in cylinder wakes, AIAA Journal 17 (9) (1979) 1012–1013.
[21] M. Braza, P. Chassaing, H.H. Minh, Prediction of large-scale features in the wake of a circular cylinder, Physics of Fluids A 2 (8) (1990) 1461–1471.
[22] G.S. Triantafyllou, M.S. Triantafyllou, C. Chryssostomidis, On the formation of vortex streets behind stationary cylinders, Journal of Fluid Mechanics 170 (1986) 461–477.
[23] F.K. Owen, D.A. Johnson, Measurements of unsteady vortex flowfields, AIAA Journal 18 (10) (1980) 1173–1179.
[24] P. Catalano, M. Wang, G. Iaccarino, P. Moin, Numerical simulation of the flow around a circular cylinder at high Reynolds numbers, International Journal of Heat and Fluid flow 24 (4) (2003) 463–469.
[25] L.F. Ryan, Experiments in aerodynamic cooling, PhD thesis, ETH, Zurich, 1951.
[26] H.C. Hottel, A. Kalitinsky, Temperature measurements in high velocity air streams, Journal of Applied Mechanics 67 (1945) A25–A32.
[27] R.J. Moffat, Gas temperature measurement, in: Temperature: its measurement and control in science and industry, Reinhold Publishing Corporation, NY, 1962, pp. 553–571.